Slow slip events and megathrust coupling changes contribute to the earthquake potential in Oaxaca, Mexico

Carlos Villafuerte[1,*], V. M. Cruz-Atienza[2], J. Tago[3], D. Solano-Rojas[3], R. Garza-Girón[4,+], S. I. Franco[2], L.A. Dominguez[2], and V. Kostoglodov[2]

[1]Laboratoire de Géologie, Département de Géosciences, École Normale Supérieure, PSL Université, CNRS UMR 8538, Paris, France

[2]Instituto de Geofísica, Universidad Nacional Autónoma de México, Mexico City, Mexico.

[3]Facultad de Ingeniería, Universidad Nacional Autónoma de México, Mexico City, Mexico.

[4]Department of Earth and Planetary Sciences, University of California, Santa Cruz, USA.

[*]Now at Instituto de Geofísica, Universidad Nacional Autónoma de México, Mexico City, Mexico.

[+]Now at Department of Geosciences, Colorado State University, Fort Collins, CO, USA

Key Points:

- Oaxaca, earthquake potential, SSE, coupling changes, La Crucecita earthquake, Coulomb stress.

Corresponding author: Carlos Villafuerte, `villafuerte.cd@gmail.com`

Summary

Stress accumulation on the plate interface of subduction zones is a key parameter that controls the location, timing and rupture characteristics of earthquakes. The diversity of slip processes occurring in the megathrust indicates that stress is highly variable in space and time. Based on GNSS and InSAR data, we study the evolution of the interplate slip-rate along the Oaxaca subduction zone, Mexico, from October 2016 through October 2020, with particular emphasis on the pre-seismic, coseismic and post-seismic phases associated with the June 23, 2020 Mw 7.4 Huatulco earthquake (also known as La Crucecita earthquake), to understand how different slip regimes contribute to the stress accumulation in the region. Our results show that continuous changes in both the aseismic stress-releasing slip and the coupling produced a high stress concentration (i.e., Coulomb Failure Stress (CFS) of 80 kPa) prior to the event on the region with the highest moment release of the Huatulco earthquake (between 17 and 30 km depth) and a stress deficit zone in the adjacent updip region (i.e., shallower than 17 km depth with CFS around -90 kPa). This region under negative stress accumulation is explained by recurrent shallow Slow Slip Events (SSE) offshore Huatulco, first reported here, as well as by the stress shadow from adjacent locked segments. These findings may explain both the main-rupture downdip propagation of the earthquake and its moderate propagation to shallower, tsunamigenic interface regions, respectively. Absent in the literature, the shallow rupture is characterized by a secondary slip patch (between 7 and 14 km depth) that overlaps with the highest concentration of aftershocks and two offshore precursor processes at the interface during the two months prior to the event, namely a Mw 5.7 shallow SSE and a rising foreshock seismicity, suggesting their involvement in the earthquake nucleation, occurred 10 km to the north. During the same period, a Mw 6.6 long-term SSE also occurred about 80 km northwest from the hypocenter, between 25 and 55 km depth. Time variations of the interplate coupling around the adjacent 1978 (Mw 7.8) Puerto Escondido rupture zone clearly correlate with the occurrence of the last three SSEs in Oaxaca far downdip of this zone, suggesting that SSEs are systematically accompanied by increasing interplate coupling transients in the shallower seismogenic zone, possibly associated with along-dip fluid diffusion at the subduction interface which in turn have their own potentially-seismogenic stress and frictional implications.Throughout the four-year period analyzed, the interface region of the 1978 event experienced a remarkably high CFS built-up of 80-150 kPa, primarily attributable to both the co-seismic and early post-seismic slip of the Huatulco rupture, indicating large earthquake potential near Puerto Escondido. Continuous

monitoring of the interplate slip-rate thus provides a better estimation of the stress accumulation in seismogenic regions than those given by long-term, time-invariant coupling models, and improves our understanding of the megathrust mechanics where future earthquakes are likely to occur.

1 Introduction

Large earthquakes along subduction zones occur in regions known as asperities (Lay & Kanamori, 1981), which represent areas of the interplate contact where frictional resistance allows elastic stress to build up during tens to hundreds of years as a consequence of the relative plate motion. Under the simple concept of Coulomb failure criterion, an earthquake occurs when the shear stress overcomes the strength of the fault. Both stressing-rate and fault strength are parameters that vary in time and space during the megathrust earthquake cycle. Therefore, understanding the tectonic and mechanical processes that cause these variations is essential to assess the seismic hazard in subduction zones.

Inter-seismic coupling maps obtained from geodetic observations have been widely used to identify heterogeneous, highly locked segments of the plate interface where large earthquakes take place (Chlieh et al., 2008; Loveless & Meade, 2011; Moreno et al., 2010; Perfettini et al., 2010). Most of these estimations consider a steady-state long term deformation during inter-seismic periods that results in a time invariant locking pattern. However, it has been observed that interplate coupling also varies with time (Heki & Mitsui, 2013; Melnick et al., 2017) and might be caused by different processes such as pore pressure transients (V. M. Cruz-Atienza et al., 2018; Materna et al., 2019; Warren-Smith et al., 2019) or dynamic stresses from regional earthquakes (V. Cruz-Atienza et al., 2021; Delorey et al., 2015; Materna et al., 2019).

During the inter-seismic period, a broad spectrum of tectonic processes occurs on the plate interface with distinctive spatiotemporal characteristics that play an important role to accommodate the strain along the megathrust. Among these processes, short-term and long-term slow slip events (SSEs), which are aseismic slip transients lasting from days to months, release the strain accumulation in the deeper and shallower segments of the plate interface (Beroza & Ide, 2011; Saffer & Wallace, 2015). Since their discovery, observations and theoretical models have shown that SSEs increase the stress in the adjacent seismogenic zone and may trigger damaging earthquakes (Obara & Kato, 2016; Segall & Bradley, 2012;

Uchida et al., 2016; Voss et al., 2018). Moreover, it has been documented that major interplate earthquakes in different subduction zones are preceded by SSEs (Kato et al., 2012; Ito et al., 2013; Socquet et al., 2017; Radiguet et al., 2016; V. Cruz-Atienza et al., 2021), although the actual mechanisms of their interaction remain under debate .

In the Mexican subduction zone, the recurrence of Mw 7+ interplate earthquakes is ~30-50 years (Singh et al., 1981). In the deeper segment of the megathrust (30-50 km depth), long-term SSEs occur in Oaxaca and Guerrero with recurrence time of ~1.5 and ~3.5 years, respectively (Cotte et al., 2009; S. Graham et al., 2016). The last five Mw 7+ interplate events in the Guerrero and Oaxaca subduction zone were preceded by SSEs in the downdip adjacent region: The 2014 Mw 7.4 Papanoa earthquake (Radiguet et al., 2016) and the 2021 Mw 7.0 Acapulco earthquake (Cruz-Atienza personal communication) in Guerrero and three more in Oaxaca, the 2012 Mw. 7.5 Ometepec earthquake (S. E. Graham et al., 2014a), the 2018 Mw 7.2 Pinotepa earthquake (V. Cruz-Atienza et al., 2021) and, as it will be shown later, the 2020 Mw 7.4 Huatulco earthquake. Although SSEs do not always trigger large earthquakes, they do interact periodically with the adjacent locked regions, thus contributing with the total stress built-up of the seismogenic zone.

Three years before the 2020 Huatulco earthquake, a complex sequence of SSEs and devastating earthquakes took place from June 2017 to July 2019 in central and southern Mexico, including the Mw 8.2 Tehuantepec and Mw 7.1 Puebla-Morelos earthquakes in 2017 (Suárez et al., 2019; Melgar et al., 2018; Mirwald et al., 2019; Singh et al., 2018) , and the Mw 7.2 Pinotepa earthquake in 2018 (Li et al., 2020), describing a cascade of events interacting with each other on a regional scale via quasi-static and/or dynamic perturbations (V. Cruz-Atienza et al., 2021).

Here we thoroughly study the evolution of the interplate slip-rate history in the Oaxaca segment during this unprecedented sequence including the pre-seismic, coseismic and post-seismic phases of the 2020 Huatulco earthquake with the aim of understanding how these processes contribute to the seismic potential in the region. We show that continuous and simultaneous monitoring of SSEs and the megathrust coupling provides a better estimation of the stress accumulation on the locked regions where future large earthquakes are expected to occur.

2 The 2020 Mw 7.4 Huatulco Earthquake

2.1 Coseismic slip inversion

On June 23, 2020, a shallow Mw 7.4 interplate thrust earthquake took place below the state of Oaxaca, Mexico (Fig. 1), with relocated hypocentral coordinates (latitude = 15.822º, longitude = -96.125º and depth = 18.2 km, determined from regional seismic records including station HUAT of the Mexican Servicio Sismológico Nacional (SSN), located 7 km south of the epicenter) within the aftershock area of the 1965 Mw 7.5 earthquake, the last interplate rupture in this region (Chael & Stewart, 1982). We combined nearfield GNSS and Interferometric Synthetic Aperture Radar (InSAR) data to determine the coseismic slip distribution by means of ELADIN, a newly developed adjoint inversion method that honors physically consistent restrictions (e.g., rake angle and von Karman slip distributions) via a gradient projection strategy (Tago et al., 2021) (see Supplementary Information).

For the GNSS data (see Supplementary Information for data processing details) we used daily averaged displacements on seven sites with epicentral distance smaller than 160 km . Three-component coseismic discontinuities in all sites were estimated independently from one-day extrapolations of two regression functions before and after the earthquake. Before the earthquake we used linear regressions over 30-day-long windows, while after the earthquake, following Savage et al. (2005) we used a logarithmic function of time of the form $A + B \log t$ to fit the data over 45-day-long windows. For both regressions the day of the earthquake was excluded, and their corresponding values extrapolated (yellow dots, Figure S1). Coseismic discontinuities, reported in Figure S1 and shown as vectors in Figure 2c, are simply the differences of the extrapolated values. At station HUAT, 7 km south of the epicenter, we found a vertical GNSS uplift of 53.2 ± 1.2 cm (Figures 2c and S1), which is consistent with an independent estimate from a collocated tide gauge recording of 49 ± 5 cm (see Figure S2 for data processing details). Seaward horizontal displacement in this site, here first reported, is 41.1 ± 0.6 cm.

For the InSAR data (see Supplementary Information for data processing details), the line-of-sight (LOS) displacement map (Figs. 2a and 2b) was generated from scenes taken before the earthquake, on June 19, and two days after the earthquake, on June 25, by the Sentinel satellite of the European Space Agency on ascending track 107, with LOS azimuth at HUAT station of 258.8º and elevation angle of 56.9º. Maximum LOS displacement of 65.3 cm was found about 10 km west from the HUAT.

For the coseismic slip inversion we assumed a planar fault discretized by 5 x 5 km^2 subelements with focal mechanism (strike = 271º, dip = 17º and rake = 70º) determined by the United States Geological Survey (USGS) through the W-phase inversion. To find the optimal data weights for the joint inversion of GNSS and InSAR data we first inverted each data set individually. Both independent solution models produced an almost perfect data fit but significantly different slip distributions, as shown in Figures S3b and S3c. Numerous joint inversion tests led us to the optimal data weights (see Supplementary Information) producing a solution that honors the most prominent features of both independent models and satisfactorily explains the whole set of observations, with average GNSS and InSAR data errors of 0.19 ± 0.26 cm and 0.63 ± 0.5cm, respectively (Figs. 2d and S3a).

Following the Mobile Checkerboard (MOC) strategy introduced by Tago et al. (2021), we performed resolution tests for the joint GNSS and InSAR inversion considering patch sizes of 21 and 30 km with a von Karman correlation length (L) of 5 km (see Supplementary Information). Our resolution analysis reveals that Average Restitution Indexes (ARI, a metric that minimize the resolution dependence on the checkerboard position) above 0.8 enclose the region where rupture took place (Fig. 3), which means that our preferred slip model (Fig. 2c) has a nominal error below 20% with respect to the actual slip distribution.

Our preferred slip solution (Fig. 2c) features a prominent slip patch slightly downdip from the hypocenter, between 15 and 25 km depth, with peak slip of 3.6 m and a second, smaller offshore patch 30 km updip from the hypocenter no yet reported in the literature, with an average slip value of 1.5 m. Our slip solution shares characteristics with previous slip models that assumed different hypocentral locations and/or focal mechanisms, such as the large downdip slip patch and the main rupture directivity towards the north-northeast, downward from the hypocenter (Melgar et al., 2021; Guo et al., 2021; Yan et al., 2022; Wen et al., 2021). However, unlike all previous solutions, our model explains well both, the uplift and seaward displacement at HUAT, the nearest GNSS station, which is critical to constrain the offshore rupture propagation (Figs. 1 and 2c). Three more features stand out from our model: 1) the updip end of the main rupture patch is very close to the nucleation point, 2) the downdip slip limit (33 km depth) might correspond to the end of the locked segment of the megathrust, as observed for the 2018 Pinotepa Earthquake (Li et al., 2020), the 2012 Ometepec Earthquake (UNAM-Seismology-Group, 2013) and the aftershocks areas of regional interplate earthquakes (e.g., the white patch of the 1965 rupture, Fig. 1), and

3) the offshore slip patch is coincident with both the highest density of aftershocks (Fig. 1) and, as we shall demonstrate below, foreshock seismicity.

2.2 The 2020 Oaxaca SSE that preceded the earthquake

Two months before the Huatulco earthquake, on mid-April 2020, three GNSS stations in Oaxaca (TNNP, TNNX and OAXA) changed their secular interseismic motion from northeast to southwest, indicating a transient deformation associated with a SSE (light blue section in Fig. 4a). We used daily continuous displacement records on 14 permanent GNSS stations in Oaxaca (Fig. 4b and 4c) belonging to the SSN and Tlalocnet (Cabral-Cano et al., 2018), between September 2019 and the Huatulco earthquake date (Fig. S4) to simultaneously invert for the plate interface coupling (PIC, i.e., 1 - v/v_{pl}, where v is the interplate slip rate, v_{pl} is the plate convergence rate and $v \leq v_{pl}$) and any stress-releasing slip episode (i.e., SSEs) in successive time windows using ELADIN (Fig. 4b-e). To this end, we carefully denoised the displacement time series by fitting and removing harmonic signals with pediods of 365 (annual), 365/2 (semi-annual), and 365/3 days related to seasonal effects and periodic GNSS constalation patters (Amiri-Simkooei et. al, JGR, 2007). Regressions of the harmonic functions were conducted following an inter-SSE multi-window strategy as detailed in the Supplementary Information (Fig. S5). For the aseismic slip inversions, we assumed the 3D plate interface geometry introduced by (V. Cruz-Atienza et al., 2021) and discretized it with subfaults of 10 x 10 km^2. Given both the interface geometry and the distribution of the GNSS stations in Oaxaca, we adopted the optimal von Karman regularization length of 40 km determined by Tago et al. (2021), which guarantees an nominal error below 50% (i.e., median restitution indexes higher than 0.5) for slip patches larger than $\sim$80 km length at most interface depths greater than 10 km (Fig. S6).

Figures 4b to 4e show the nine-month evolution of the long-term SSE (O-SSE3), which initiated in a shallow region close to the 2018 (Mw 7.2) Pinotepa earthquake hypocenter, migrated downdip and then along-strike to the east, where the main dislocation patch took place in the last two months prior to the earthquake downdip of the 1978 Puerto Escondido earthquake region, between 25 and 55 km depth, and with cumulative moment magnitude Mw 6.6 (Mo = 10.23 x 10^{18} N*m measured from the slip contour of 0.5 cm and assuming a shear modulus of 32 GPa), which is smaller than the two previous SSEs in Oaxaca of 2017-2018 (O-SSE1) and 2019 (O-SSE2) with Mw 6.9 (Table 1; (V. Cruz-Atienza et al., 2021)). The location of this SSE, however, is consistent with previous events in the region

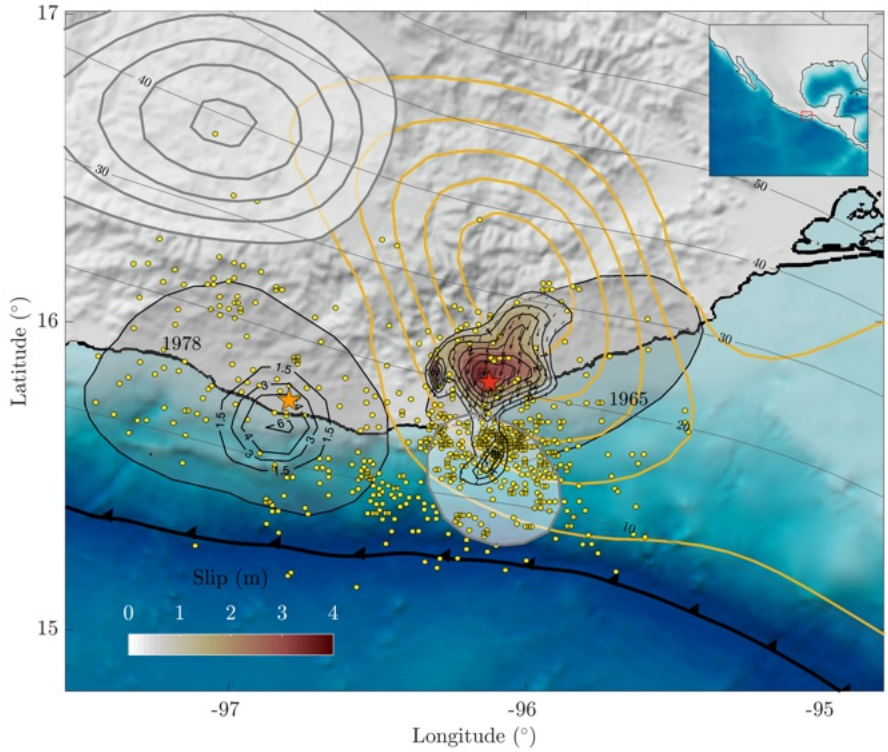

Figure 1. Study region and slip inversions for pre-seismic, coseismic and post-seismic phases of the 2020 Mw 7.4 Huatulco earthquake. Red colored region with black contours indicates the slip on the plate interface for our preferred joint GPS and InSAR coseismic slip inversion. White shaded patches with gray contours indicate the downdip and shallow SSE that took place before the event with slip isolines every 1 cm beginning with 0.5 cm. Yellow contours depict the afterslip following the Huatulco event with slip isolines every 10 cm beginning with 5.0 cm. Red and orange stars indicate the epicenters of the Huatulco and the 1978 Puerto Escondido earthquakes, respectively. Black contours around the 1978 Puerto Escondido epicenter represent the slip isolines (in m) determined by Mikumo et al. (2002). Dark gray shaded patches show the aftershock areas of the historic thrust earthquakes of 1965 and 1978. Yellow dots depict the first 50 days Huatulco earthquake aftershocks reported by the SSN. Gray contours indicate the iso-depths (in km) of the 3D plate interface used for the slip inversions in this study.

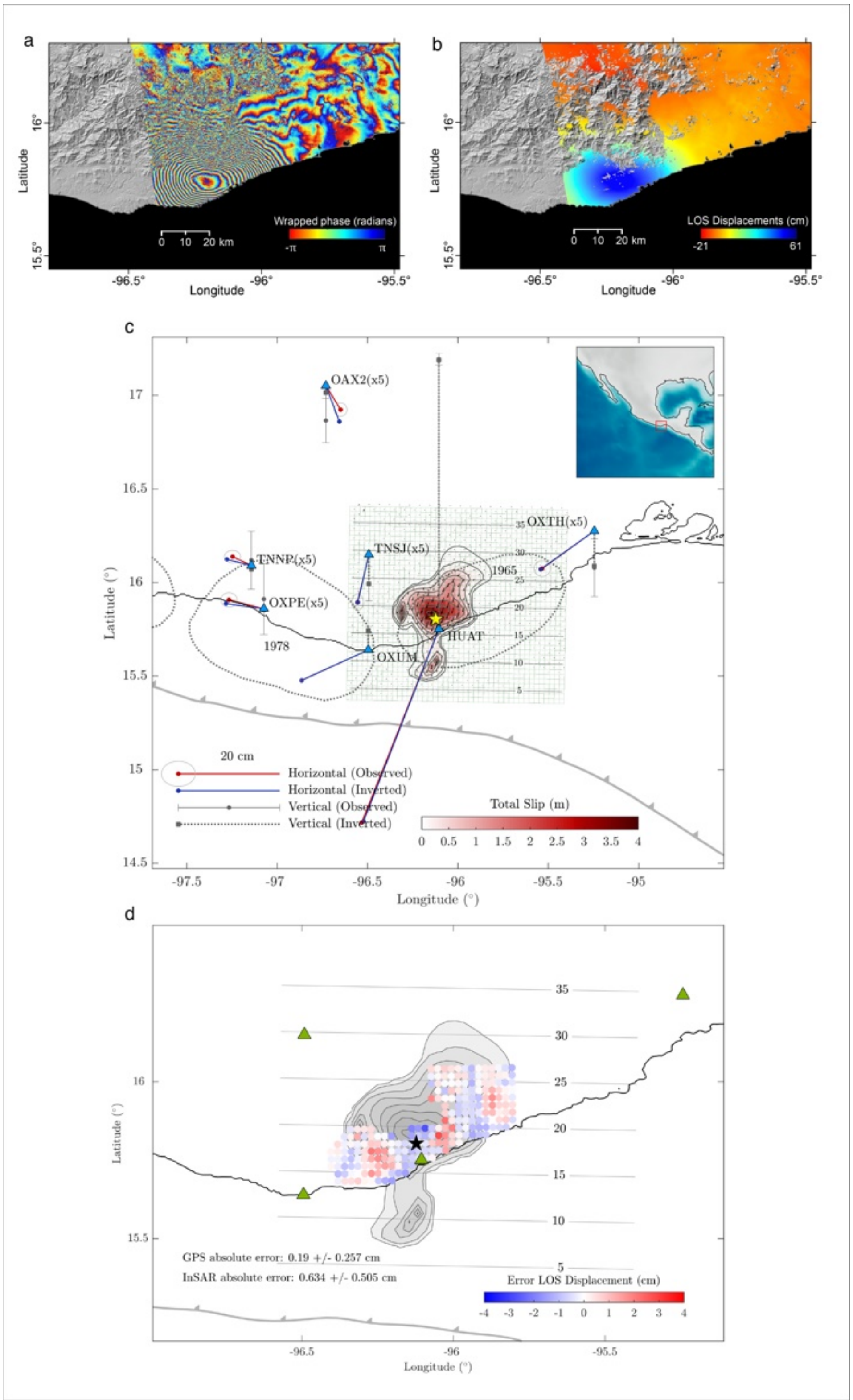

Figure 2. Coseismic slip of the Huatulco earthquake and GNSS and InSAR data used for the inversion. **a** Wrapped phase ascending interferogram estimated from Sentinel satellite images on Track 107 Ascending for scenes on June 19 and 25, 2020. **b** Line of sight (LOS) displacement from ascending track, positive values correspond to motion towards the satellite. **c** Joint slip inversion with the observed and predicted displacements in the seven GNSS stations. **d** Misfit between observed and predicted LOS surface displacements for our preferred slip model.

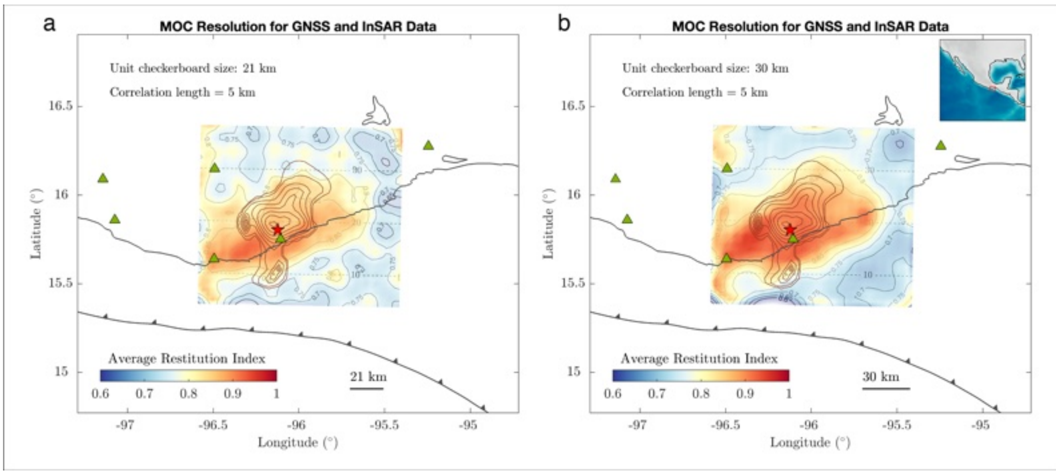

Figure 3. Resolution analysis for the coseismic GNSS+InSAR joint inversion. Average restitution index (ARI) obtained from a mobile checkerboard (MOC) analysis that integrates 64 independent checkerboard inversions with patch sizes (PS) of **a** 21km and **b** 30 km using a correlation length (L) of 5 km. Green triangles are the GNSS stations. Gray contours show our preferred slip model for the 2020 Huatulco earthquake and the yellow star the epicenter.

(Correa-Mora et al., 2008; V. Cruz-Atienza et al., 2021; S. Graham et al., 2016). The SSE clearly did not penetrate the rupture area of the Huatulco earthquake. However, in the same nine-month period, at least two short-term, shallow SSEs occurred offshore from the hypocenter of the 2021 Huatulco earthquake, the second clearly seen on Figure 4e with moment magnitude Mw 5.7. As we shall demonstrate later in Section 3, this offshore segment in Oaxaca is prone to recurrent aseismic events.

A careful one-station template-matching analysis of the foreshock seismicity within 30 km from the hypocenter using continuous three-component broadband records at station HUAT (i.e., SSN station HUIG) (V. Cruz-Atienza et al., 2021; Garza-Girón et al., 2023) starting from August 2016 revealed a sustained growth in the seismicity rate during the six months prior to the earthquake (completeness magnitude Mc = 2.0; Figure S7c) in the same offshore region where the short-term SSEs were taking place. When compared to Figure S7a, the inset in Figure 4e reveals that the seismicity rate increased in the year prior to rupture, concentrating mainly in the shallow, locked asperity of the earthquake, a few kilometers south of the hypocenter. Something similar occurred in the hypocentral region of the 2018 Pinotepa earthquake (Mw 7.2) 200 km west, where the seismicity rate close to the hypocenter also increased during the O-SSE1 in the two months preceding the rupture (V. Cruz-Atienza et al., 2021). As shown in Figure 1, the shallow coseismic asperity is also found just in the offshore segment where most of the aftershocks occurred. All these observations along with the shallow afterslip propagation (introduced in next section) feature a very active, potentially tsunamigenic interface region nearby Huatulco where slow and fast earthquakes cohabitate and support our capability to resolve short-term SSEs from GNSS data in this offshore region of Oaxaca.

On the other hand, Figures 4b to 4e further reveal a noteworthy PIC evolution prior to rupture around the Huatulco earthquake hypocentral region, where the interface decoupled around February-March (Fig. 4d) before getting fully coupled the two months before the earthquake (i.e., during the strongest SSE phase, Fig. 4e). This can also be seen directly in the GNSS time series at the stations closest to the epicenter, such as OXUM and HUAT (Fig. 4a), where we do not see the SSE southward rebound. Although the transient deformation produced by the SSE is clear from mid-April, the inter-SSE displacement trends in some stations far from the coast started changing well before, around mid-February as shown in Figure 4a (red dashed lines), revealing a gradual plate interface decoupling process at a regional scale preceding the main SSE-induced crustal relaxation (Figures 4b-d and 4f). Before the decoupling process began (Fig. 4b), the downdip segment of the plate interface, between 25-50 km, was fully coupled. Figures 4d and 4f further show how the segment downdip of the 1978 earthquake area (dotted circle) is the last one to experience a PIC drop (i.e., the interface slip accelerates but remains below the plate convergence rate) leading to the forthcoming main SSE dislocation patch on April-June, the months preceding the Huatulco earthquake (Figs. 4e and 4f). The cummulative seismic moment of such event corresponds to Mw 6.6, which is 0.3 units lower than the 2017 (O-SSE1) and 2019 (O-SSE2) SSEs (Table 1).These observations highlight the regional-wide preparatory phase for the 2020 Oaxaca SSE and, possibly, of the main shock.

A common practice to isolate the deformation associated with slow slip transients is to subtract the inter-SSE linear trend from the GNSS time series. The residual deformation is then assumed to correspond to the strain released by the SSE. When doing this to invert for the slip at the interface, the preparatory phase of the SSE (i.e., the slow decoupling process preceding the SSE relaxation) is mapped and interpreted as aseismic slip resulting in an overall elastic crustal rebound (i.e., a stress drop). However, since this process instead reveals a gradual decrease in the upper crustal stressing rate (red dashed lines in Figure 4a), such a misleading practice leads to a systematic overestimation of the SSE-related surface displacements and, therefore, of the SSE equivalent seismic moment with relevant implications in the slip budget over several SSE cycles, which may be significantly misestimated. This has been also pointed out previously by Ochi and Kato (2013) in the Tokai region in Central Japan.

2.3 Early post-seismic deformation

We inverted the early post-seismic GNSS displacements (i.e., the first 4 months following the earthquake discretized in 8 fifteen-day windows, yellow dots in Figures 5a and S8b) produced by the mainshock using the same parametrization for the ELADIN method as in the previous section, yielding a total scalar moment of 1.084x10^{20} Nm and Mw 7.3, which is close to the Mw 7.2 afterslip of the 2018 Pinotepa earthquake (Table 1). We then assumed that such displacements are only due to the afterslip on the plate interface, which is a reasonable approximation considering that the viscoelastic relaxation after a similar thrust event 260 km west, the 2012 (Mw 7.5) Ometepec earthquake, was negligible in a six month post-seismic period (S. E. Graham et al., 2014b).

Three main observations arise from the afterslip evolution of the Huatulco earthquake (Fig. 5b): 1) the largest slip concentrates between 20 and 50 km depth barely reaching the main SSE patch preceding the earthquake (i.e., downdip from the 1978 rupture area) and overlapping the 2017 and 2019 SSEs (V. Cruz-Atienza et al., 2021) (OSSE-1 and OSSE-2 in Fig. 6a); 2) the main afterslip area completely overlaps with the coseismic rupture area; 3) the afterslip spreads offshore towards the oceanic trench where short-term SSEs occurred before the earthquake and where the foreshocks and aftershocks concentrated.

The complete overlap of coseismic and postseismic slip has been observed in the last three interplate thrust earthquakes (Mw 7) in Oaxaca, the 2012 (Mw 7.5) Ometepec (S. E. Graham et al., 2014b); the 2018 (Mw 7.2) Pinotepa (V. Cruz-Atienza et al., 2021) and the 2020 (Mw 7.4) Huatulco (this study) events, indicating that these seismogenic segments of the plate interface, with depth range between 10 and 30 km, can release elastic strain energy both seismically and aseismically. However, the propagation of the Huatulco earthquake afterslip to the trench is an interesting feature that clearly differs from the 2018 Pinotepa earthquake, whose afterslip stopped under the coast (i.e., at ∼15 km depth and without offshore propagation, see next section) (Figs. 6a and S9e-g). This observation suggests significant lateral variations in the geometrical and/or mechanical characteristics along

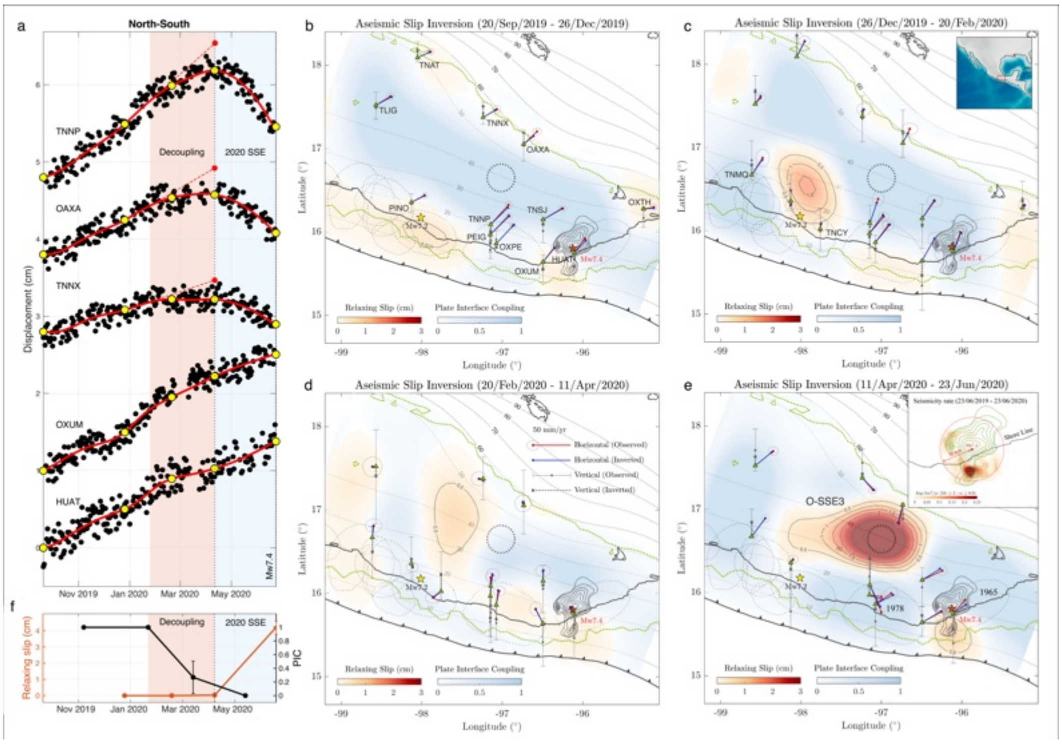

Figure 4. GNSS inversions of the 9-month deformation period prior to the June 23, 2020, Mw 7.4 Huatulco earthquake. **a** North-south GNSS time series in 5 selected stations. Yellow dots indicate the beginning and end of the four time-windows used for the slip inversions shown in **b- e**, and red dashed lines depict the inter-SSE displacement trend during the interface decoupling phase. **b- e** Inverted slip in the plate-convergence (PC) direction for all time windows. Inset of panel **e** shows the template-matching foreshocks seismicity rate 12 months preceding the earthquake. Slip contours are in centimeters. Red and yellow stars indicate the epicenters of the Huatulco and 2018 Pinotepa (Mw 7.2) earthquakes, respectively. Dashed regions are the aftershock areas of historic interplate earthquakes. Gray ellipses around the arrow tips are represent one standard deviations of the observed displacements. **f** Average and standard deviation (vertical bars) of the plate interface coupling (PIC) and relaxing slip in the region where the 2020 SSE developed (i.e., within the dotted black circle in **b- e**).

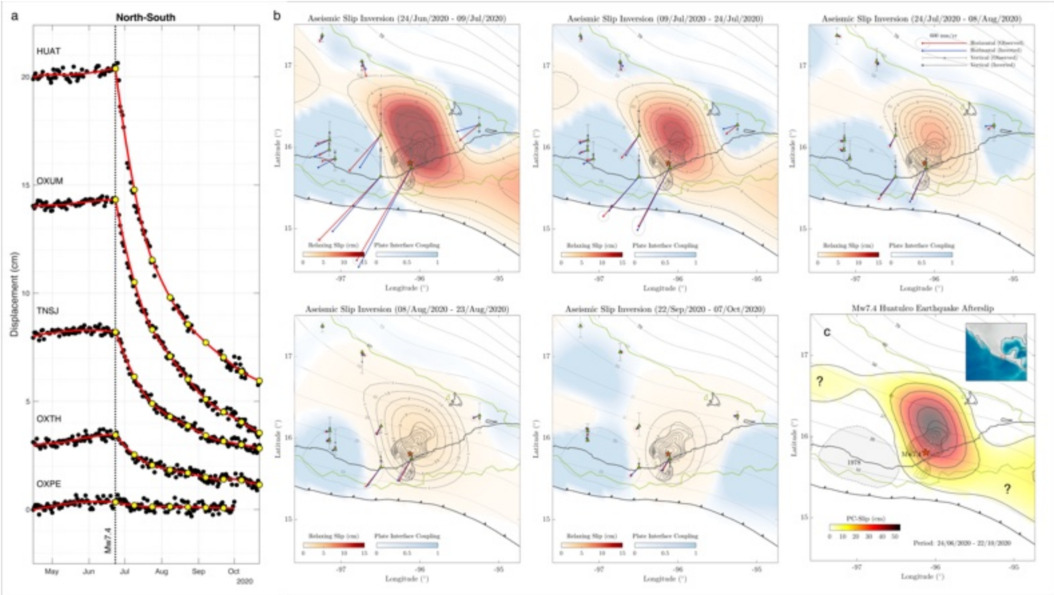

Figure 5. GNSS inversion of the postseismic deformation of the Huatulco earthquake. **a** North-south displacement GNSS time series in 5 selected stations. Yellow dots indicate the start and the end of the six 15-day windows used for the slip inversions, some of them shown in **b** (notice the dates in every panel). **b** Aseismic slip evolution for the postseismic phase of the Huatulco earthquake.Thick light gray contours are the coseismic slip shown in figure 2a. c Cumulative afterslip during the four months following the earthquake.

the Oaxaca subduction zone, especially in the shallow, potentially tsunamigenic interface region.

Another noteworthy feature of the postseismic process in the region is that the Huatulco earthquake postslip did not penetrate the rupture area of the 1978 Puerto Escondido earthquake (dashed ellipse in Figs. 5b-c), which remained fully coupled during the four-month period. Unlike most of the preseismic phase, the PIC in the 1978 rupture area remained fully locked after the earthquake (compare Figs. 4 and 5) suggesting significant dynamic implications for the accommodation of postseismic strain in the region.

3 Interplate slip-rate evolution in the Oaxaca subduction zone.

Before the occurrence of the Huatulco earthquake, a complex sequence of SSEs and earthquakes took place in an unusual way along the Mexican subduction zone from April 2017 to September 2019 due to the extremely large, unprecedented seismic waves from

Table 1. Dates and magnitudes of all Slow Slip Events in Oaxaca from June 2017 to June 2020, as well as the afterslip of the 2018 Mw 7.2 Pinotepa (PE-afterslip) and 2020 Mw 7.4 Huatulco (HE-afterslip) earthquakes.

Events	Dates	Mw
O-SSE1*	01/06/2017 – 15/02/2018	6.9
PE-Afterslip*	16/02/2018 – 22/11/2018	7.2
O-SSE2*	16/02/2018 – 22/11/2018	6.9
O-SSE3+	26/12/2019 – 23/06/2020	6.6
HE-Afterslip+	23/06/2020 – 22/10/2020	7.3

* From Cruz-Atienza et al. (2021). , + This study

the Mw 8.2 Tehuantepec earthquake on September 8, 2017 (V. Cruz-Atienza et al., 2021). During this period, two large SSEs occurred in the downdip interface region of Oaxaca (namely the 2017 SSE (O-SSE1) and the 2019 SSE (O-SSE2)) where the recent 2020 SSE (O-SSE3) took also place (Figure 6a and Table 1). In fact, the plate interface slipped aseismically and continuously for two years from O-SSE1, experiencing two spontaneous reactivations in this period, one before the Pinotepa earthquake and the other with the O-SSE2 (V. Cruz-Atienza et al., 2021).

We corrected the GNSS displacement time series used by V. Cruz-Atienza et al. (2021) for seasonal effects from October 2016 to September 2019 as previously done in section 2.2 (Fig. S5) and reinverted them for the interplate aseismic slip in detail along the Oaxaca megathrust using the 17 GNSS stations. The new inverted sequence is shown in Figure S9. During the sequence, the plate interface experienced remarkable changes of the PIC over time in the whole megathrust. To analyze the long-term evolution of the aseismic slip before the Huatulco earthquake, we integrated the new corrected slip sequence from October 2016 to September 2019 (Fig. S9) and the following sequence discussed in section 2.2 (from September 2019 to June 2020, Fig. 4), and linearly interpolated the complete slip history every 30 days. We also decomposed the total slip into relaxing and stressing interface regions, i.e., into SSEs and afterslip regions where the slip rate is greater than the plates convergence rate and, therefore, relax elastic strain (e.g. red gradient zones in Figs. 4, 5 and S9); and regions under coupling regime, where the velocity of the interplate creep is less than or equal to the plates convergence rate, which increases eastward along the coast

(DeMets et al., 2010) and, therefore, accumulate elastic strain (e.g. blue gradient zones in Figs. 4, 5 and S9).

Figure 6 shows the evolution of the cumulative relaxing slip until the day before the Huatulco earthquake (i.e., projected onto the green line of Figure 6a) averaged in two different depth ranges, between 10-20 km depth (Fig. 6b) and between 20-30 km depth (Fig. 6c), encompassing the rupture areas of the 2018 Pinotepa, 1978 Puerto Escondido and 2020 Huatulco earthquakes (Fig. 6a). Figures 6b and 6c show that the Pinotepa earthquake afterslip (yellow areas) dominates in the region for the analyzed period. However, as mentioned earlier, there are other significant slip episodes (i.e., short-term SSEs) often observed in the shallow zone (within the 10-20 km depth range), abscent in the 1978 rupture segment, where at least four SSEs offshore Huatulco took place accumulating in 3.5 years a total slip of 3 cm.

To better examine the interplate slip-rate variations we averaged the slip at six different locations on the plate interface to analyze its temporal evolution. These locations are denoted by dashed blue circles in Figure 6a, each having a radius of 20 km. We categorized these locations based on their depth: the first group, DS, corresponds to deeper regions spanning 20-30 km, while the second group, SS, is associated with shallower areas ranging from 10-20 km in depth. Region DS-1 is located over the main rupture area of the Huatulco earthquake; Region SS-2, over the rupture area of the 1978 Puerto Escondido earthquake as estimated by Mikumo et al. (2002); Region DS-2, downdip from the rupture area of the Puerto Escondido earthquake; Region SS-1, updip from the Huatulco earthquake where most of its foreshocks and aftershocks occurred; and Regions SS-3 and DS-3, west and northwest of the Puerto Escondido earthquake. Figures 7 and S10 show the evolution of the relaxing slip (red line) and the PIC (blue line) within each of the six regions.

The Huatulco rupture area (Fig. 7a; region DS-1) is mainly characterized by PIC variations in the whole analyzed period. Slip relaxation took place only in a period after the Mw 8.2 Tehuantepec earthquake, when aseismic stress release occurred during the late phase of the O-SSE1 (see Figures 6a and S10c). This phase of the O-SSE1 was indeed triggered by the quasistatic and dynamic stresses produced by the great Tehuantepec event as demonstrated by V. Cruz-Atienza et al. (2021). We also find a gradual four-month decrease of PIC down to 0.1-0.2 at the end of the afterslip period of the Pinotepa earthquake that eventually recovers during the O-SSE2 to remain high (around 0.8) high until the Huatulco earthquake occurs.

In the 1978 rupture area (Region SS-2, Fig. 7b) there is no significant evidence of aseismic stress release (red line), so that the region slips mostly as creep. In this seismogenic region, PIC changes (blue line) correlate remarkably well with the occurrence of downdip SSEs in Oaxaca (gray rectangles) even though these events did not penetrate the shallow region. During the SSEs, PIC gradually increases to values of 0.7-0.8 in the initial stage of every SSE and then decreases in their final stage to remain relatively low, with values down to 0.2-0.4 observed during the inter-SSE periods. This remarkable behavior, which suggests a non-intuitive interaction between deep SSEs and the coupling regime in the shallower seismogenic zone, is also found in Region SS-3 (Fig. S10b), west of the 1978 rupture area.

To the east and thus offshore (and updip) the Huatulco earthquake (Region SS-1, Fig. S10a) we find a different and more consistent low PIC value across the whole studied period (between 0 and 0.3) with the exception of a prominent increase after the Tehuantepec earthquake, which might be associated with the stress shadow produced in this specific spot by the great Mw8.2 rupture (Suárez et al., 2019; V. Cruz-Atienza et al., 2021). As pointed out earlier for this region, the red curve indicates that there are small and persistent short-term, episodic SSEs in this offshore region over time that can also be appreciated in Figures 4b-e and 6b. Such a particular aseismic slip behavior is consistent with the significant afterslip that swept that shallow area close to the trench after the Huatulco earthquake (Fig. 5). These observations along with the Huatulco earthquake offshore propagation suggest that mechanical properties of this offshore region are prone to release seismically and aseismically the accumulated tractions, as recently found in the western segment of the Guerrero seismic gap (Plata-Martínez et al., 2021).

Finally, downdip from the 1978 rupture area (Regions DS-2 and DS-3, Figs. S10c and S10d) we observe a highly variable PIC evolution because of its proximity to the deep SSEs region. During the occurrence of SSEs, PIC reductions begin well before the silent events, meaning that creeping in some subfaults of these regions gradually accelerates before reaching the plates convergence velocity and thus initiating the stress drop (see how the blue curves start decreasing before the red curves start growing). These observations also indicate that SSEs might partly penetrate these deep seismogenic regions (20 -30 km depth) (see also Figure 6a).

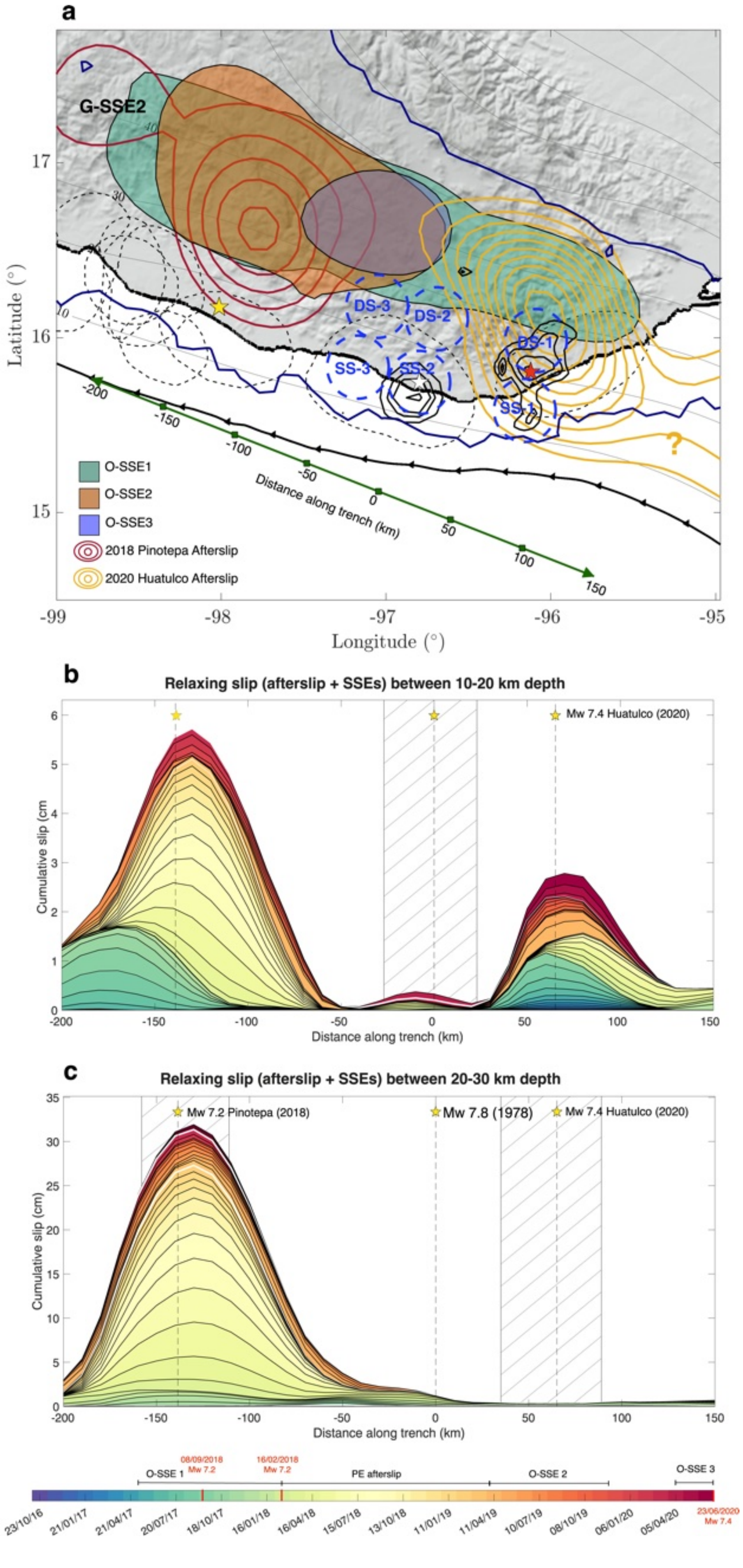

Figure 6. (Caption next page.)

Figure 6. Aseismic slip at the plate interface in Oaxaca. **a** Summary of the aseismic slip processes (SSEs and afterslip) occurring from October 2016 to August 2020 in Oaxaca. Colored patches indicate the SSEs regions with slip values higher than 2.0 cm. Colored contours depict the afterslip of the Pinotepa and Huatulco earthquakes with slip isolines every 5 cm beginning with 5 cm. Dark blue contour indicates the region with restitution indexes higher than 0.5 from Figure S6b. Red, orange and yellow stars indicate the hypocenter of the Huatulco, the 1978 Puerto Escondido and the Pinotepa earthquakes, respectively. Dashed blue circles represents the areas where we analyze the evolution of the interplate slip rate and the CFS shown in Figs. 7 and S10. Green line indicates the along-trench profile where the evolution of the aseismic slip and CFS on the plate interface is analyzed in b and c and Figs. 8 and 9. **b** and **c** show the evolution of the relaxing aseismic slip (SSEs and afterslip) along the trench within the seismogenic zone averaged between 20-30 and 10-20 km depth, respectively. Hatched regions show the interplate segments with the highest moment release of the 2018 Pinotepa, 1978 Puerto Escondido and 2020 Huatulco earthquakes. Stars and dashed black lines indicate the along-trench coordinate of the hypocenters.

4 Implications of SSEs and PIC changes on the stress built-up

We estimated the CFS changes (Nikkhoo and Walter (2015), see Section 4 of the Supplementary Information) produced by the relaxing slip (SSEs and afterslip) and the interplate coupling to elucidate how the stress evolves along the Oaxaca segment. For this analysis we have also included the coseismic stress changes produced by the Tehuantepec (V. Cruz-Atienza et al., 2021), Pinotepa (Li et al., 2020) and Huatulco earthquakes. Figure 8 show the cumulative CFS every 30 days from October 2016 up to the Huatulco event on June 2020 along the trench (i.e., projected onto the green line in Figure 6a) averaged on two different depth ranges encompassing the main rupture areas of the 2018 Pinotepa and 2020 Huatulco earthquakes (between 20 and 30 km depth, Fig. 8a) and the 1978 Puerto Escondido (between 10 and 20 km depth, Fig. 8b) earthquake. One should bear in mind that these estimates of the CFS are the result of stress contributions from the whole plate interface and not just from the sub-faults delimited by the corresponding depth ranges.

For the deeper region (Fig. 8a), we observe that despite the large variations of the slip-rate discussed above on the megathrust, the CFS in Huatulco always increased up to values ranging from 60 to 80 kPa. We also observe a CFS contribution of $\sim$10 kPa induced by the Mw8.2 Tehuantepec earthquake in the eastern limit of the Huatulco rupture zone

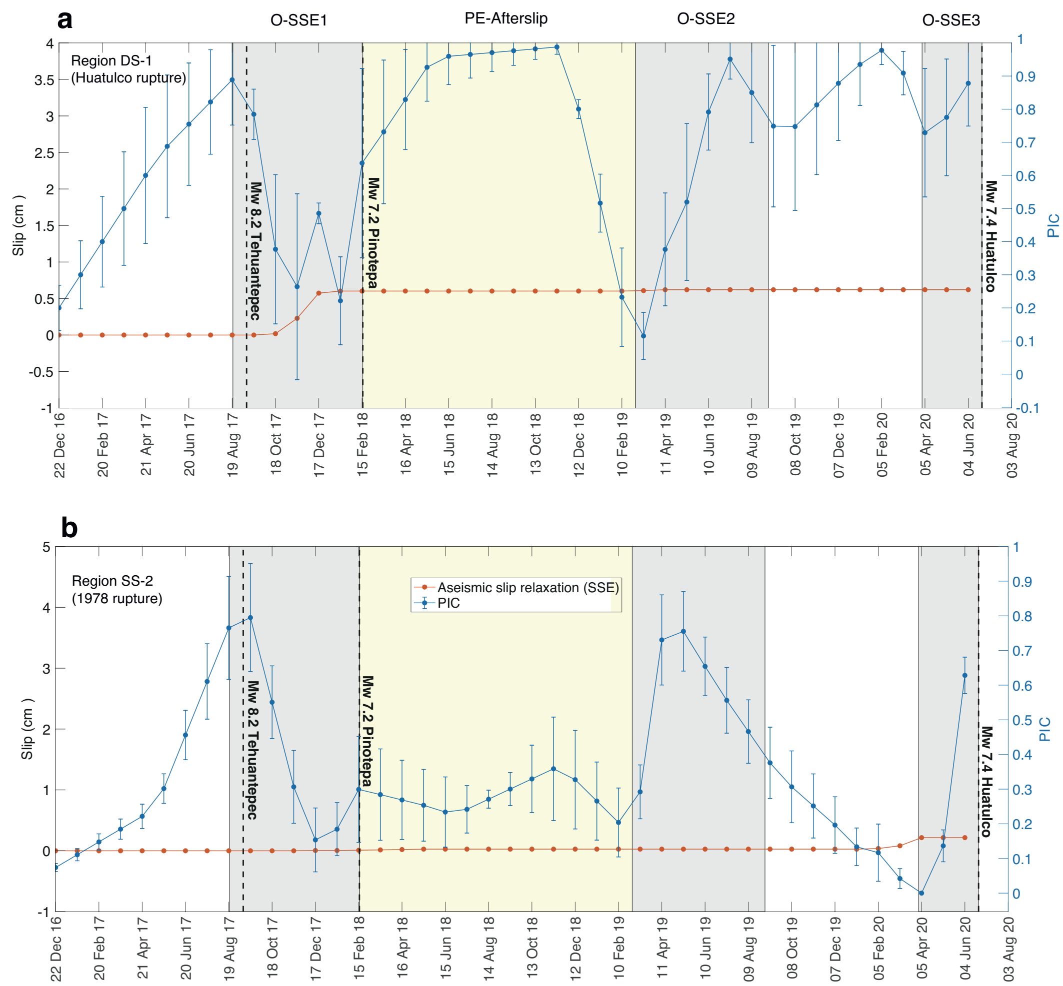

Figure 7. Detailed evolution of the aseismic slip in the seismogenic segment of Oaxaca. Time series show the cumulative total slip, creeping (slip under coupling regime), relaxing slip (SSEs) and plate interface coupling (PIC) in **a** Region A (the Huatulco rupture area) and **b** Region B (the 1978 Puerto Escondido rupture area) (see Figure 4). Gray rectangles indicate the time windows of the downdip SSEs in Oaxaca. The light-yellow rectangle depicts the timespan of the 2018 Pinotepa earthquake afterslip in the region.

that exceeds 30 kPa further to the east. For the shallower region (Fig. 8b), the CFS systematically decreases and remains negative right updip of the Huatulco rupture reaching values of ∼-90 kPa. This negative CFS is associated with both the stress shadows produced by neighboring coupled segments and the periodic stress release by short-term SSEs in this offshore segment (Fig. 6b).

Figure S11 shows both the long-term and inter-SSE time-invariant interplate coupling models estimated by Radiguet et al. (2016, personal communication) (left column) together with their associated CFS change rate (right column). Both models produce large stressing rates mainly in the coupled segment of the 1978 earthquake region. However, they also produce large stress shadows in the adjacent, less coupled regions (both along-dip and along-strike) such as in the Pinotepa and Huatulco rupture zones. Although these time-invariant coupling models may lack some observational coverage compared to the present investigation, they share similar features found by Rousset et al. (2016) for the inter-SSE regime, which incorporates all available GPS observations in the region (compare Figure S11c and Figure 3B of Rousset et al. (2016)) and with the more recent short term coupling estimation by Maubant et al. (2022).

In contrast, our time-evolving aseismic slip model predicts a different scenario. Figure 9a shows the cumulative CFS at the time of the Huatulco earthquake including contributions of all aseismic slip processes imaged in the megathrust preceding the event from October 2016 to June 23, 2020 (blue areas). A simple inspection reveals large differences in the stress build-up pattern with respect to the time-invariant models (Fig. S11), especially in both the Huatulco and Pinotepa rupture areas, and east-southeast of the 1978 earthquake zone. The bottom four panels of Figure 9 show the cumulative (trench-perpendicular average) CFS along the trench for the same two depth ranges analyzed earlier. The left column shows the cumulative CFS at the time of the Huatulco earthquake, while the right column shows the same quantity plus its coseismic and postseismic stress increments (see also Fig. 9d).

In the deeper region at the moment and within the rupture area of the Huatulco earthquake (Fig. 9b), the CFS from our time-evolving slip model (blue area) indicates more than double the CFS predicted by the inter-SSE coupling model by Radiguet et al. (2016, personal communication) (yellow area), while their long-term coupling model (orange area) predicts even negative CFS values (i.e., no earthquake potential). Downdip of the 1978 rupture area, the CFS predicted by the three models are consistent (values ranging be-

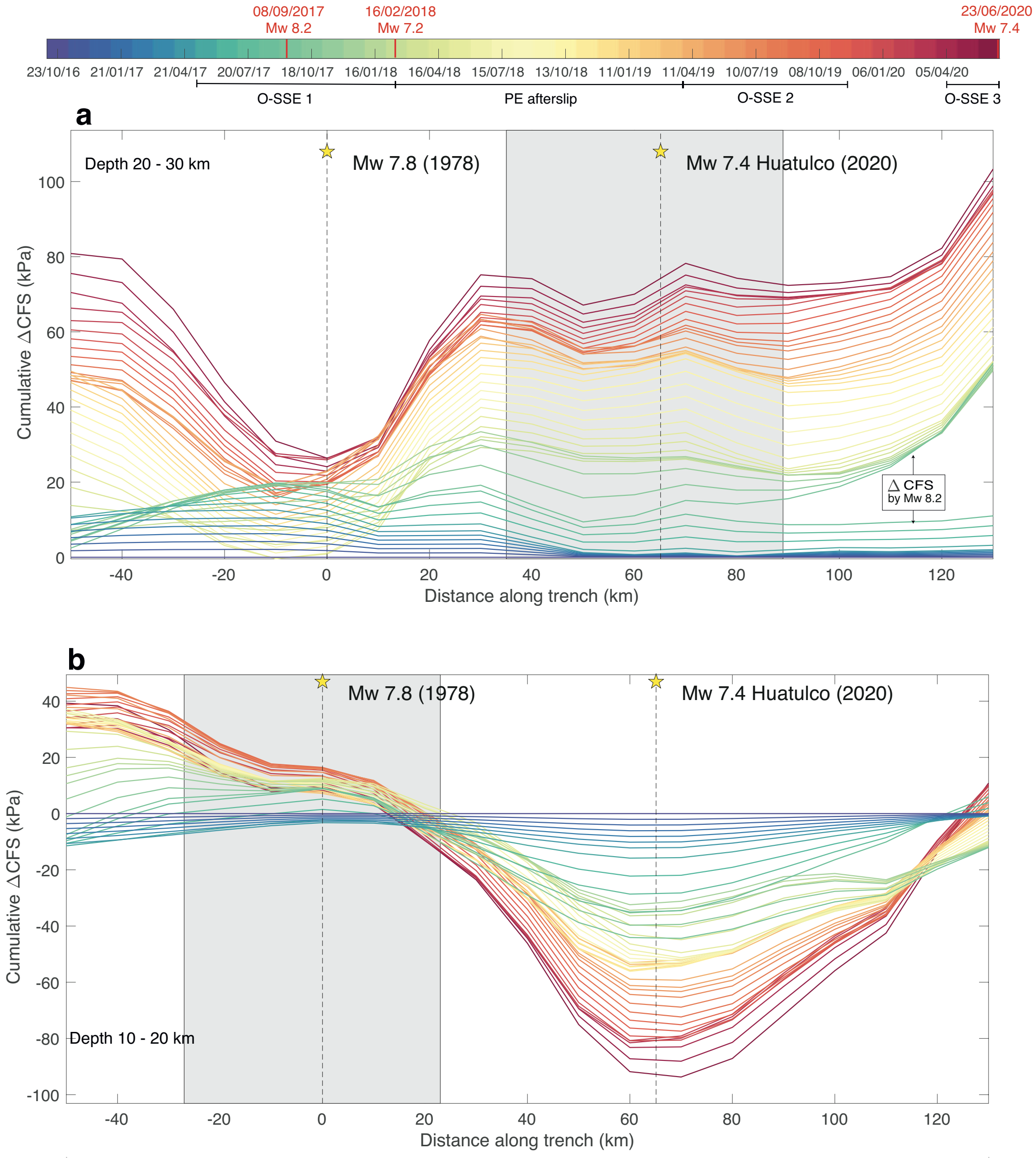

Figure 8. Evolution of the CFS in the seismogenic segment of Oaxaca. Evolution of the total CFS along the trench for every 30 days averaged between **a** 20-30 km and **b** 10-20 km depth. Gray rectangles show the interplate segments with the highest moment release of the 2020 Huatulco earthquake and the 1978 Puerto Escondido event (Mikumo et al., 2002).

tween 20 and 30 kPa), but to the west of this region our model again predicts very different stress concentrations, which are twice the CFS predicted by the inter-SSE coupling model of Radiguet et al. When adding the CFS imparted by the Huatulco earthquake and its postseismic slip shown in Figure 9d, our estimate abruptly increases right downdip of the 1978 rupture area, from about 30 kPa to over 130 kPa. A significant fraction of this value is due to the persistently high coupling in this region throughout the post-seismic phase (Fig. 5). This large, relatively deep segment west of the Huatulco rupture (Region DS-2 in Fig. 6a) might be then highly prone to a future earthquake, as has happened in neighbouring regions over the deep part of the locked zone where the last two interplate earthquakes in Oaxaca (the Pinotepa and Huatulco events) took place, with most of their seismic moment released below 15 km (Fig. 1a and Li et al. (2020)).

In the shallower region (Fig. 9c), the time-invariant coupling models predict higher CFS values overall than our time-evolving slip model before the Huatulco earthquake, including the 1978 rupture area. Only when adding the coseismic and postseismic stresses induced by the 2020 earthquake, the inter-SSE model prediction by Radiguet et al. becomes similar to ours in the eastern part of the rupture area of the 1978 Puerto Escondido earthquake (Fig. 9f). Only our time-evolving model predicts a large CFS deficit updip of the Huatulco rupture area, which is fully compensated (reaching positive values around 70 kPa) by the coseismic and postseismic deformations produced by the Huatulco earthquake (Figs. 9d and 9f).

In summary, we can therefore distinguish three major differences between our time-evolving CFS estimates and those from the time-invariant coupling models introduced by Radiguet et al. : (1) a high stress concentration over the main downdip rupture area of the Huatulco earthquake before the event predicted only by our model, (2) except for the 1978 rupture segment, absolute CFS values between 20 and 30 km depth are at least twice as high in our model, and (3) a large stress deficit zone updip the Huatulco rupture before the event that is absent in both time-invariant models.

Figures 10a and 10b show separately the overall CFS contributions of both the slip under coupling regime and the relaxing slip, respectively, during the whole analyzed period before the Huatulco earthquake. Although in different proportions, both stress contributions increase the earthquake potential in the main rupture areas of the Huatulco and 1978 earthquakes. Figures 10c and 10d visually depict the percentage ratio of these contributions

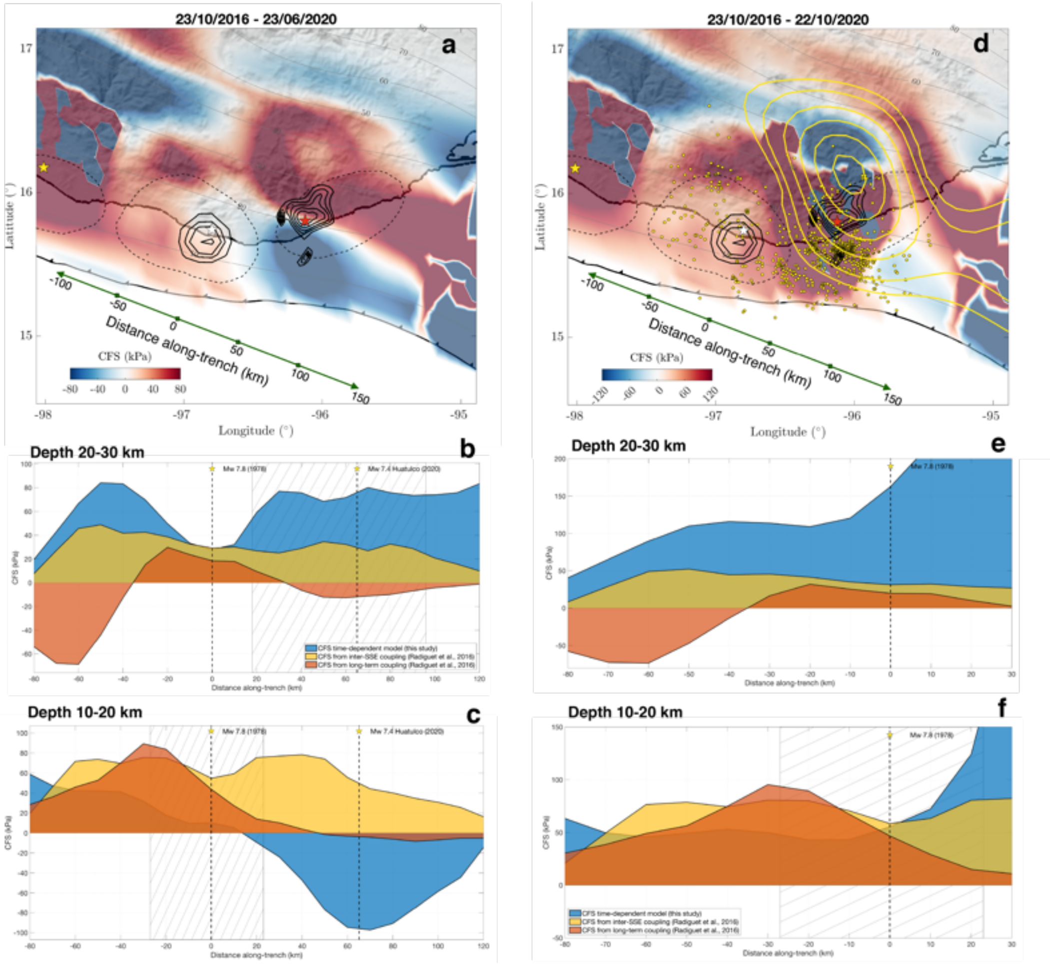

Figure 9. Cumulative CFS from the time-variant model and its comparison with the stress built up predicted by time-invariant coupling models. **a** Cumulative CFS in the plate interface between October 2016 and the date of the 2020 Huatulco earthquake. Black contours represent the isoslip values for the 2020 Huatulco and 1978 Puerto Escondido (Mikumo et al., 2002) earthquakes. Black dashed lines delimit the aftershock areas of historic interplate earthquakes. White dashed circles represent the regions where we analyze the evolution of the interplate slip rate and the CFS shown in figures 6, 7c and 7d. **b** and **c** Comparison between our cumulative CFS time-variant model and the CFS predicted by time-invariant coupling models of the region between October 2016 and the date of the 2020 Huatulco earthquake for two depth bands, between 20-30 km depth and between 10-20 km depth, respectively. **d** Same than a but including the stress contributions from the coseismic and postseismic phases of the Huatulco earthquake. Yellow contours are the 5,10,20 and 30 cm slip isolines of the two months cumulative afterslip. Yellow dots depict the 50 days aftershocks after the Huatulco Earthquake reported by the SSN. **e** and **f** Same as **b** and **c** but including the stress contribution from the coseismic and postseismic phases of the Huatulco earthquake focused only in the 1978 rupture segment.

to the overall CFS (as displayed in Fig. 9a). This analysis is limited to regions displaying positive CFS values, which means to areas with effective seismogenic potential.

Between 20-30 km depth (regions DS-1 and DS-2), we observe that most of the accumulated stress (∼65-80%) was generated by coupled interface regions (Fig. 10c) and the remaining ∼20-35% by the relaxing slip (i.e., long- and short-term SSEs, and the Pinotepa earthquake afterslip) (Fig. 10d) which frequently occurred in the region during more than 3.5 years (Figs. S12a and S12b). Given its proximity with the Pinotepa earthquake, Region DS-3 differs significantly from this stress partitioning pattern because it is strongly affected by the stresses produced during the coseismic slip and afterslip of the event (Fig. S12c). The shallower, offshore Region SS-1, which has no prestress earthquake potential, experienced a sustained reduction of CFS due to both coupling-related stress shadows (Fig. 10a) and short-term SSEs (Fig. 10b) in similar proportions (Fig. S12d).This analysis demostrates the highly heterogeneous stress accumulation and partitioning along the plate interface in the Oaxaca segment.

5 Discussion

Previous M7 class interplate earthquakes in Oaxaca such as those of 1965 and 1928 occurred in close proximity of the 2020 Huatulco rupture, suggesting a possible reactivation of the same asperity over time (Chael & Stewart, 1982; Singh et al., 1984). Historical data also suggest that two older, probably thrust earthquakes with magnitude larger than 7 occurred nearby in 1870 and 1801 (Suárez et al., 2020). Assuming that all these events broke the same plate interface asperity, their average return period would be 55 +/- 13 years.

In this Oaxaca region, the great Mw ∼8.6 San Sixto earthquake ruptured a ∼300 km along-strike segment in 1787 producing a very large tsunami offshore Oaxaca (Suárez & Albini, 2009; Ramírez-Herrera et al., 2020). Such event must have involved several locked segments along the Oaxaca megathrust, including shallow portions of the plate interface to generate the mega-tsunami. Whether M8+ events may repeat depends, among other factors, on the interplate mechanical properties and constructive stress interaction between different locked and unlocked fault areas (Kaneko et al., 2010, 2018), which evolve with time and may escape from the quantitative analysis of known seismicity over the last century (Nocquet et al., 2017). To have an insight into the actual megathrust earthquake potential, i.e., to

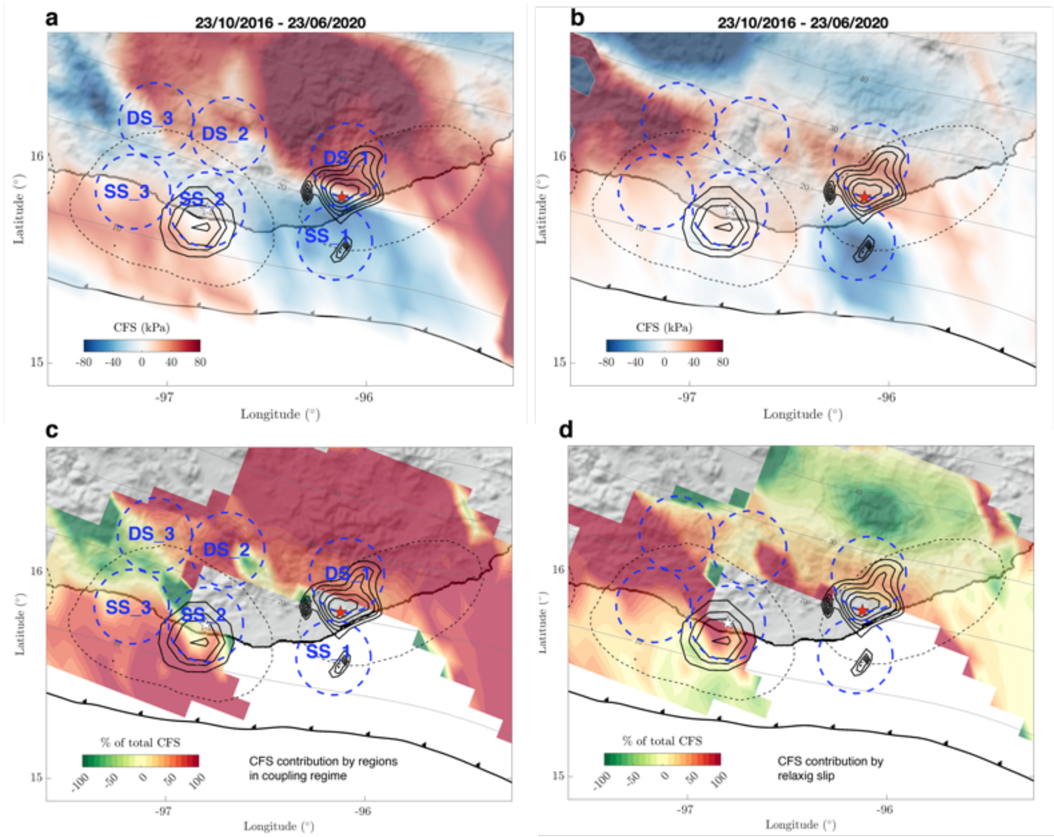

Figure 10. CFS contributions by regions in coupling regime and relaxing slip. **a** and **b** show the cumulative CFS contributions in the plate interface between October 2016 and the date of the 2020 Huatulco earthquake associated with regions in coupling regime and relaxing slip, respectively. **c** and **d** show the CFS contributions (in %) on the plate interface where the total CFS is positive (see figure 7a) by regions in coupling regime and relaxing slip, respectively

assess whether adjacent locked segments are likely to break jointly to produce a much larger event, it is thus necessary to quantify the stress accumulation throught continuous data assimilation as proposed here. Monitoring the interplate slip-rate continuously might also allow us to constrain the evolution of frictional parameters that control the fault stability conditions along the complex geometry of the megathrust.

An interesting feature of the Huatulco earthquake is that rupture mainly propagated downdip, without significant slip in the adjacent updip segment (above ∼15 km depth). Impeding a large rupture into this shallower segment might be partly explained with the existence of the stress barrier produced by both the stress shadow from nearby coupled zones and persistent shallow short-term SSEs (see Figures 6b and 9a). However, other factors such as the geometry of the interface (e.g. subducted plate reliefs in the region, as recently proposed in the Guerrero seismic gap (Plata-Martínez et al., 2021)) and frictional variations could also contribute to the explanation of this particular rupture pattern. Also interesting is the earthquake initiation at the shallowest extremity of the main asperity and its northward propagation. The nucleation point lies between a highly stressed (downdip) and a highly relaxed (updip) interface regions (Fig. 9a), which means on a place with relatively large stress gradient and, therefore, deformation. The initiation of the earthquake at this point is therefore reasonably explained by our model, as is its main propagation towards the most loaded, downdip interface region.

Our results also suggest that the interplate coupling in Oaxaca is variable in space and time (Figs. 7, S9 and S10). Such remarkable PIC variations might certainly be related with changes in the mechanical properties of the fault zone materials induced by the dynamic perturbations of seismic waves from recent significant regional earthquakes (V. Cruz-Atienza et al., 2021; Materna et al., 2019; Delorey et al., 2015). Particularly interesting are the PIC variations in the shallow, seismogenic zone (i.e., between 10 and 20 km depth), which seems to be somehow linked to the occurrence of deeper, long-term SSEs (Figs. 7b and S10c). To explain these PIC variations at shallow depths we favor the idea involving transient fluctuations of fluid pressure at the interface, as proposed for the long-term SSEs in the Guerrero (V. M. Cruz-Atienza et al., 2018), southern Cascadia (Materna et al., 2019), Japan (Bedford et al., 2020) and Hikurangi (Warren-Smith et al., 2019) subduction zones. Recent models evoking the fault-valving concept show that overpressure fluid pulses migrate along the subduction channel as the permeability evolves in the fault zone due to slow deformation processes (V. M. Cruz-Atienza et al., 2018; Shapiro et al., 2018; Zhu et al., 2020; Farge et al., 2021). These transient changes in pore pressure may lead to large variations of the fault strength as high as ∼10-20 MPa (Zhu et al., 2020), which makes this mechanism a plausible candidate to explain the strong and systematic PIC variations we found in the shallow seismogenic zone of Oaxaca during the occurrence of SSEs downdip.

Earthquake potential depends on the state of stress along the subduction zone which, as shown here, is a function of different evolving processes taking place from the trench to its deep portion. The stress build-up therefore changes over time and space in a complex way, so does the earthquake potential. Time-invariant estimates of the interplate coupling are often used to identify seismogenic segments prone to large earthquakes (Chlieh et al., 2008; Loveless & Meade, 2011; Moreno et al., 2010; Perfettini et al., 2010). However, while these estimates are certainly useful on a large spatial and temporal scale, they do not allow a reliable picture of the earthquake potential associated with smaller ($7 < M < 8.5$) but potentially devastating ruptures that occur more frequently, as shown in this work for the Oaxaca megathrust.

Our results indicate that continuous and systematic monitoring of the interplate slip velocity, incorporating simultaneously the stressing (i.e., coupled) and relaxing (i.e., slow, coseismic and postseismic) slip regimes in a continuum, provides a more reliable reconstruction of the short-term stress evolution over the megathrust and, probably also, of the long-term evolution which, together with a seismic monitoring of tectonic tremor and repeating earthquakes, could provide significant insights into the M8+ earthquake supercycles. Proceeding this way may thus be relevant to evaluate theoretical predictions of the interface dynamics, which is our leading approach to understand the underlying physics in subduction systems.

6 Conclusions

We analyzed the interplate slip-rate evolution during more than 3.5 years in the Oaxaca subduction zone including the preseismic, coseismic and postseismic phases associated with the June 23, 2020 Mw 7.4 Huatulco earthquake to better understand how the different slip regimes contribute to the plate-interface stress accumulation and thus to the seismogenic potential. We found that the rupture area of the Huatulco earthquake extends between 7 and 33 km depth with a main, compact slip patch around 15 to 25 km depth north-northeast from the hypocenter and a second, much smaller shallow patch offshore and south from the hypocenter where recurrent short-term SSEs occur, including a Mw 5.7 during the two months prior to the rupture about 10 km south of the hypocenter. This finding along with the colocated foreshock seismicity, aftershocks and shallow afterslip feature a very active, potentially tsunamigenic interface region close to Huatulco where slow and fast earthquakes cohabitate. Such prominent coseismic subevent offshore was not reported in previous investigations likely due to the lack of the well-resolved 3D displacement vector next to the hypocenter at the SSN station HUAT, first used here. The entire rupture zone falls within the aftershock area of the 1965 Ms 7.2 earthquake, suggesting rupture of the same or a very close asperity. The long-term, Mw 6.6 SSE that occurred downdip before the earthquake did not penetrate the rupture area and was preceded by a gradual interface decoupling process at a regional scale, including the maximum SSE slip area. During the two months preceding the earthquake, when the strongest phase of the 2020 SSE developed downdip, the Huatulco earthquake rupture area became fully locked. Our slip inversions indicate that the four-month earthquake afterslip overlapped the whole coseismic rupture area and propagated both to the trench, where the foreshocks and most of aftershocks happened, and downdip to the north, where the 2020 SSE was developing. During the post-seismic phase, the rupture area of the 1978 Puerto Escondido earthquake became and remained fully coupled.

The interplate slip-rate evolution in Oaxaca during the 3.5 years preceding the Huatulco earthquake shows that PIC in the megathrust seismogenic region is highly variable in time and space. One prominent feature of such variations is a clear correlation between transient PIC increments at shallow depths (10-20 km, including the 1978 rupture area) and the occurrence of three successive SSEs far downdip, suggesting a physical interaction likely related to fluid diffusion at the interface induced by aseismic slip processes in nearby regions that simultaneously relax and load different interface sections.We also found that both relaxing aseismic slip events and megathrust coupling changes during those 3.5 years produced a significant stress concentration ($\sim$80 kPa) downdip the region of the Huatulco earthquake nucleation zone likely promoting the main downdip rupture of the event. Furthermore, these stress contributions produced as well a large and shallow (offshore) stress reduction ($\sim$-90 kPa) that may have impeded (along with other possible factors) a much larger updip propagation of the earthquake with tsunamigenic potential.

Our results indicate that continuous monitoring of the interplate aseismic slip-rate and its CFS counterpart provide a better estimation of M7+ earthquake potential over seismogenic regions than predictions yielded by time-independent interplate coupling models.

Finally, the stress imparted during the coseismic and postseismic phases of the Huatulco earthquake on the 1978 Puerto Escondido rupture area (and its downdip portion between 20 and 30 km depth) makes it a region prone to the another earthquake in the near future, a forecast consistent with the ∼55 years return period in this Oaxaca region.

Declaration on competing or conflict of interest

The authors have no competing or conflict of interest in what is expressed in this manuscript.

Data availability Part of the GPS data analyzed in this study are available under some restrictions in the repository of the "Servicio Sismológico Nacional de la UNAM" (http:// www.ssn.unam.mx). Broadband seismic data is publicly available in the same repository. Part of the GPS data in the state of Oaxaca are available in the repository of the "TLALOCNet del Instituto de Geofísica de la UNAM" (http://tlalocnet.udg.mx). The rest of the GPS data in the state of Guerrero are not publicly available until March 2026 due to the restriction policies of the SATREPS-UNAM research project. For more information contact the corresponding author.

Code availability Custom computer programs and mathematical algorithms that are deemed central to the conclusions of this study are available on request from the corresponding author.

Acknowledgments

We are grateful for the outstanding technical support of Eduardo Murrieta and Luciano Díaz in the maintenance of the Gaia supercomputing platform, and Luis Salazar in the TLALOCNet field operations and stations maintenance. We thank Mathilde Radiguet for kindly providing us the long-term coupling models. We also thank Shri Krishna Singh, Arturo Iglesias and Gerardo Suárez for fruitful discussion; the Servicio Sismológico Nacional (SSN), the Servicio Mareográfico Nacional (SMN) and the Servicio de Geodesia Satelital, all of them from the Instituto de Geofísica-UNAM, for all GNSS, strong motion and tide gauge data, as well as all their personnel for data acquisition and distribution; and the European Space Agency for access to the Sentinel1 data. This work is partially based on GNSS data belonging also to TLALOCNet and services provided by the GAGE Facility, operated by UNAVCO, Inc., with support from the National Science Foundation and the National Aeronautics and Space Administration under NSF Cooperative Agreement EAR-1724794. All GNSS data has been processed in the Laboratorio de Geodesia Satelital (LaGeos) of the Instituto de Geofísica-UNAM. This work was supported by CONACyT grants 6471 and 255308, UNAM-PAPIIT grants IN113814, IG100617 and IG100921, JICA-JST SATREPS-UNAM grant 15543611, UNAM-DGTIC grant LANCAD-312 and the graduate school scholarships by CONACyT. CV was supported by the European Research Council grant PERSISMO (grant 865411).

CRediT authorship contribution statement

C. Villafuerte: Conceptualization, Methodology, Investigation, Formal Analysis, Writing-Original Draft, Visualization. **V.M. Cruz-Atienza**: Conceptualization, Methodology, Investigation, Visualization, Writing-Review and Editing, Supervision. **J. Tago**: Methodology, Investigation, Software, Validation, Review and Editing. **D. Solano-Rojas**: Investigation, Validation, Data processing, Review and Editing **R. Garza-Girón**: Investigation, Visualization, Data processing, Review and Editing **S.I. Franco**: Data processing, Editing. **L.A. Dominguez**: Investigation, Editing. **V. Kostoglodov**: Investigation, Review and Editing.

References

Bedford, J. R., Moreno, M., Deng, Z., Oncken, O., Schurr, B., John, T., ... Bevis, M. (2020). Months-long thousand-kilometre-scale wobbling before great subduction earthquakes. *Nature*, *580*(7805), 628–635.

Beroza, G. C., & Ide, S. (2011). Slow earthquakes and nonvolcanic tremor. *Annual review of Earth and planetary sciences*, *39*, 271–296.

Cabral-Cano, E., Pérez-Campos, X., Márquez-Azúa, B., Sergeeva, M., Salazar-Tlaczani, L., DeMets, C., ... others (2018). Tlalocnet: A continuous gps-met backbone in mexico for seismotectonic and atmospheric research. *Seismological Research Letters*, *89*(2A), 373–381.

Chael, E. P., & Stewart, G. S. (1982). Recent large earthquakes along the middle american trench and their implications for the subduction process. *Journal of Geophysical Research: Solid Earth*, *87*(B1), 329–338.

Chlieh, M., Avouac, J.-P., Sieh, K., Natawidjaja, D. H., & Galetzka, J. (2008). Heterogeneous coupling of the sumatran megathrust constrained by geodetic and paleogeodetic measurements. *Journal of Geophysical Research: Solid Earth*, *113*(B5).

Correa-Mora, F., DeMets, C., Cabral-Cano, E., Marquez-Azua, B., & Diaz-Molina, O. (2008). Interplate coupling and transient slip along the subduction interface beneath oaxaca, mexico. *Geophysical Journal International*, *175*(1), 269–290.

Cotte, N., Walpersdorf, A., Kostoglodov, V., Vergnolle, M., Santiago, J.-A., & Campillo, M. (2009). Anticipating the next large silent earthquake in mexico. *Eos, Transactions American Geophysical Union*, *90*(21), 181–182.

Cruz-Atienza, V., Tago, J., Villafuerte, C., Wei, M., Garza-Girón, R., Dominguez, L., ... others (2021). Short-term interaction between silent and devastating earthquakes in mexico. *Nature communications*, *12*(1), 2171.

Cruz-Atienza, V. M., Villafuerte, C., & Bhat, H. S. (2018). Rapid tremor migration and pore-pressure waves in subduction zones. *Nature communications*, *9*(1), 1–13.

Delorey, A. A., Chao, K., Obara, K., & Johnson, P. A. (2015). Cascading elastic perturbation in japan due to the 2012 mw 8.6 indian ocean earthquake. *Science advances*, *1*(9), e1500468.

DeMets, C., Gordon, R. G., & Argus, D. F. (2010). Geologically current plate motions. *Geophysical Journal International*, *181*(1), 1–80.

Farge, G., Jaupart, C., & Shapiro, N. M. (2021). Episodicity and migration of low frequency earthquakes modeled with fast fluid pressure transients in the permeable subduction interface. *Journal of Geophysical Research: Solid Earth*, *126*(9), e2021JB021894.

Garza-Girón, R., Brodsky, E. E., Spica, Z. J., Haney, M. M., & Webley, P. W. (2023). A specific earthquake processing workflow for studying long-lived, explosive volcanic eruptions with application to the 2008 okmok volcano, alaska, eruption. *Journal of Geophysical Research: Solid Earth*, *128*(5), e2022JB025882. Retrieved from https://agupubs.onlinelibrary.wiley.com/doi/abs/10.1029/2022JB025882 (e2022JB025882 2022JB025882)

Graham, S., DeMets, C., Cabral-Cano, E., Kostoglodov, V., Rousset, B., Walpersdorf, A., ... Salazar-Tlaczani, L. (2016). Slow slip history for the mexico subduction zone: 2005 through 2011. In *Geodynamics of the latin american pacific margin* (pp. 3445–3465). Springer.

Graham, S. E., DeMets, C., Cabral-Cano, E., Kostoglodov, V., Walpersdorf, A., Cotte, N., ... Salazar-Tlaczani, L. (2014a). Gps constraints on the 2011–2012 oaxaca slow slip event that preceded the 2012 march 20 ometepec earthquake, southern mexico. *Geophysical Journal International*, *197*(3), 1593–1607.

Graham, S. E., DeMets, C., Cabral-Cano, E., Kostoglodov, V., Walpersdorf, A., Cotte, N., ... Salazar-Tlaczani, L. (2014b). Gps constraints on the m w= 7.5 ometepec earthquake sequence, southern mexico: Coseismic and post-seismic deformation. *Geophysical Journal International*, *199*(1), 200–218.

Guo, R., Yang, H., Zhu, Y., Zheng, Y., Xu, J., Zhang, L., & An, C. (2021). Narrow rupture of the 2020 m w 7.4 la crucecita, mexico, earthquake. *Seismological Society of America*, *92*(3), 1891–1899.

Heki, K., & Mitsui, Y. (2013). Accelerated pacific plate subduction following interplate thrust earthquakes at the japan trench. *Earth and Planetary Science Letters*, *363*, 44–49.

Ito, Y., Hino, R., Kido, M., Fujimoto, H., Osada, Y., Inazu, D., ... others (2013). Episodic slow slip events in the japan subduction zone before the 2011 tohoku-oki earthquake. *Tectonophysics*, *600*, 14–26.

Kaneko, Y., Avouac, J.-P., & Lapusta, N. (2010). Towards inferring earthquake patterns from geodetic observations of interseismic coupling. *Nature Geoscience*, *3*(5), 363–369.

Kaneko, Y., Wallace, L. M., Hamling, I. J., & Gerstenberger, M. C. (2018). Simple physical model for the probability of a subduction-zone earthquake following slow slip events and earthquakes: Application to the hikurangi megathrust, new zealand. *Geophysical Research Letters*, *45*(9), 3932–3941.

Kato, A., Obara, K., Igarashi, T., Tsuruoka, H., Nakagawa, S., & Hirata, N. (2012). Propagation of slow slip leading up to the 2011 mw 9.0 tohoku-oki earthquake. *Science*, *335*(6069), 705–708.

Lay, T., & Kanamori, H. (1981). An asperity model of large earthquake sequences. *Earthquake Prediction*.

Li, Y., Shan, X., Zhu, C., Qiao, X., Zhao, L., & Qu, C. (2020). Geodetic model of the 2018 m w 7.2 pinotepa, mexico, earthquake inferred from insar and gps data. *Bulletin of the Seismological Society of America*, *110*(3), 1115–1124.

Loveless, J. P., & Meade, B. J. (2011). Spatial correlation of interseismic coupling and coseismic rupture extent of the 2011 mw= 9.0 tohoku-oki earthquake. *Geophysical Research Letters*, *38*(17).

Materna, K., Bartlow, N., Wech, A., Williams, C., & Bürgmann, R. (2019). Dynamically triggered changes of plate interface coupling in southern cascadia. *Geophysical Research Letters*, *46*(22), 12890–12899.

Maubant, L., Radiguet, M., Pathier, E., Doin, M.-P., Cotte, N., Kazachkina, E., & Kostoglodov, V. (2022). Interseismic coupling along the mexican subduction zone seen by insar and gnss. *Earth and Planetary Science Letters*, *586*, 117534.

Melgar, D., Pérez-Campos, X., Ramirez-Guzman, L., Spica, Z., Espíndola, V. H., Hammond, W. C., & Cabral-Cano, E. (2018). Bend faulting at the edge of a flat slab: The 2017 mw7. 1 puebla-morelos, mexico earthquake. *Geophysical Research Letters*, *45*(6), 2633–2641.

Melgar, D., Ruiz-Angulo, A., Pérez-Campos, X., Crowell, B. W., Xu, X., Cabral-Cano, E., … Rodriguez-Abreu, L. (2021). Energetic rupture and tsunamigenesis during the 2020 m w 7.4 la crucecita, mexico earthquake. *Seismological Society of America*, *92*(1), 140–150.

Melnick, D., Moreno, M., Quinteros, J., Baez, J. C., Deng, Z., Li, S., & Oncken, O. (2017). The super-interseismic phase of the megathrust earthquake cycle in chile. *Geophysical Research Letters*, *44*(2), 784–791.

Mikumo, T., Yagi, Y., Singh, S. K., & Santoyo, M. A. (2002). Coseismic and postseismic stress changes in a subducting plate: Possible stress interactions between large interplate thrust and intraplate normal-faulting earthquakes. *Journal of Geophysical Research: Solid Earth*, *107*(B1), ESE–5.

Mirwald, A., Cruz-Atienza, V. M., Díaz-Mojica, J., Iglesias, A., Singh, S. K., Villafuerte, C., & Tago, J. (2019). The 19 september 2017 (m w 7.1) intermediate-depth mexican earthquake: A slow and energetically inefficient deadly shock. *Geophysical Research Letters*, *46*(4), 2054–2064.

Moreno, M., Rosenau, M., & Oncken, O. (2010). 2010 maule earthquake slip correlates with pre-seismic locking of andean subduction zone. *Nature*, *467*(7312), 198–202.

Nikkhoo, M., & Walter, T. R. (2015). Triangular dislocation: an analytical, artefact-free solution. *Geophysical Journal International*, *201*(2), 1119–1141.

Nocquet, J.-M., Jarrin, P., Vallée, M., Mothes, P., Grandin, R., Rolandone, F., … others (2017). Supercycle at the ecuadorian subduction zone revealed after the 2016 pedernales earthquake. *Nature Geoscience*, *10*(2), 145–149.

Obara, K., & Kato, A. (2016). Connecting slow earthquakes to huge earthquakes. *Science*, *353*(6296), 253–257.

Ochi, T., & Kato, T. (2013). Depth extent of the long-term slow slip event in the tokai district, central japan: A new insight. *Journal of Geophysical Research: Solid Earth*, *118*(9), 4847–4860.

Perfettini, H., Avouac, J.-P., Tavera, H., Kositsky, A., Nocquet, J.-M., Bondoux, F., ... others (2010). Seismic and aseismic slip on the central peru megathrust. *Nature*, *465*(7294), 78–81.

Plata-Martínez, R., Ide, S., Shinohara, M., Mortel, E. S. G., Mizuno, N., Ramirez, L. A. D., ... Yamada, T. (2021). Shallow slow earthquakes to decipher future catastrophic earthquakes in the guerrero seismic gap. *Accepted at Nature Communications*.

Radiguet, M., Perfettini, H., Cotte, N., Gualandi, A., Valette, B., Kostoglodov, V., ... Campillo, M. (2016). Triggering of the 2014 m w 7.3 papanoa earthquake by a slow slip event in guerrero, mexico. *Nature Geoscience*, *9*(11), 829–833.

Ramírez-Herrera, M.-T., Corona, N., Cerny, J., Castillo-Aja, R., Melgar, D., Lagos, M., ... others (2020). Sand deposits reveal great earthquakes and tsunamis at mexican pacific coast. *Scientific Reports*, *10*(1), 1–10.

Rousset, B., Lasserre, C., Cubas, N., Graham, S., Radiguet, M., DeMets, C., ... others (2016). Lateral variations of interplate coupling along the mexican subduction interface: Relationships with long-term morphology and fault zone mechanical properties. *Pure and Applied Geophysics*, *173*(10), 3467–3486.

Saffer, D. M., & Wallace, L. M. (2015). The frictional, hydrologic, metamorphic and thermal habitat of shallow slow earthquakes. *Nature Geoscience*.

Savage, J. C., Svarc, J. L., & Yu, S.-B. (2005). Postseismic relaxation and transient creep. *Journal of Geophysical Research: Solid Earth*, *110*(B11). Retrieved from https://agupubs.onlinelibrary.wiley.com/doi/abs/10.1029/2005JB003687 doi: https://doi.org/10.1029/2005JB003687

Segall, P., & Bradley, A. M. (2012). Slow-slip evolves into megathrust earthquakes in 2d numerical simulations. *Geophysical Research Letters*, *39*(18).

Shapiro, N. M., Campillo, M., Kaminski, E., Vilotte, J.-P., & Jaupart, C. (2018). Low-frequency earthquakes and pore pressure transients in subduction zones. *Geophysical Research Letters*, *45*(20), 11–083.

Singh, S., Astiz, L., & Havskov, J. (1981). Seismic gaps and recurrence periods of large earthquakes along the mexican subduction zone: A reexamination. *Bulletin of the* *seismological Society of America*, *71*(3), 827–843.

Singh, S., Dominguez, T., Castro, R., & Rodriguez, M. (1984). P waveform of large, shallow earthquakes along the mexican subduction zone. bulletin of the seismological society of america. *Bulletin of the seismological Society of America*, *74*(6), 2135-2156.

Singh, S., Reinoso, E., Arroyo, D., Ordaz, M., Cruz-Atienza, V., Pérez-Campos, X., … Hjörleifsdóttir, V. (2018). Deadly intraslab mexico earthquake of 19 september 2017 (m w 7.1): Ground motion and damage pattern in mexico city. *Seismological Research Letters*, *89*(6), 2193–2203.

Socquet, A., Valdes, J. P., Jara, J., Cotton, F., Walpersdorf, A., Cotte, N., … Norabuena, E. (2017). An 8 month slow slip event triggers progressive nucleation of the 2014 chile megathrust. *Geophysical Research Letters*, *44*(9), 4046–4053.

Suárez, G., & Albini, P. (2009). Evidence for great tsunamigenic earthquakes (m 8.6) along the mexican subduction zone. *Bulletin of the Seismological Society of America*, *99*(2A), 892–896.

Suárez, G., Ruiz-Barón, D., Chico-Hernández, C., & Zúñiga, F. R. (2020). Catalog of preinstrumental earthquakes in central mexico: epicentral and magnitude estimations based on macroseismic data. *Bulletin of the Seismological Society of America*, *110*(6), 3021–3036.

Suárez, G., Santoyo, M. A., Hjorleifsdottir, V., Iglesias, A., Villafuerte, C., & Cruz-Atienza, V. M. (2019). Large scale lithospheric detachment of the downgoing cocos plate: The 8 september 2017 earthquake (mw 8.2). *Earth and Planetary Science Letters*, *509*, 9–14.

Tago, J., Cruz-Atienza, V. M., Villafuerte, C., Nishimura, T., Kostoglodov, V., Real, J., & Ito, Y. (2021). Adjoint slip inversion under a constrained optimization framework: Revisiting the 2006 guerrero slow slip event. *Accepted at Geophysical Journal International*.

Uchida, N., Iinuma, T., Nadeau, R. M., Bürgmann, R., & Hino, R. (2016). Periodic slow slip triggers megathrust zone earthquakes in northeastern japan. *Science*, *351*(6272), 488–492.

UNAM-Seismology-Group. (2013). Ometepec-pinotepa nacional, mexico earthquake of 20 march 2012 (mw 7.5): A preliminary report. *Geofísica Internacional*, *52*(2), 173–196.

Voss, N., Dixon, T. H., Liu, Z., Malservisi, R., Protti, M., & Schwartz, S. (2018). Do slow slip events trigger large and great megathrust earthquakes? *Science advances*, *4*(10), eaat8472.

Warren-Smith, E., Fry, B., Wallace, L., Chon, E., Henrys, S., Sheehan, A., … Lebedev, S. (2019). Episodic stress and fluid pressure cycling in subducting oceanic crust during slow slip. *Nature Geoscience*, *12*(6), 475–481.

Wen, Y., Xiao, Z., He, P., Zang, J., Liu, Y., & Xu, C. (2021). Source characteristics of the 2020 m w 7.4 oaxaca, mexico, earthquake estimated from gps, insar, and teleseismic waveforms. *Seismological Society of America*, *92*(3), 1900–1912.

Yan, Z., Xiong, X., Liu, C., & Xu, J. (2022). Integrated analysis of the 2020 m w 7.4 la crucecita, oaxaca, mexico, earthquake from joint inversion of geodetic and seismic observations. *Bulletin of the Seismological Society of America*, *112*(3), 1271–1283.

Zhu, W., Allison, K. L., Dunham, E. M., & Yang, Y. (2020). Fault valving and pore pressure evolution in simulations of earthquake sequences and aseismic slip. *Nature communications*, *11*(1), 1–11.